Optical and Sensing Properties of 1-Pyrenecarboxylic Acid-Functionalized Graphene Films Laminated on Polydimethylsiloxane Membranes

Xiaohong An,*,† Thomas W. Butler,‡ Morris Washington,§ Saroj K. Nayak,§ and Swastik Kar*,†

†Department of Physics, Northeastern University, Boston, Massachusetts 02115, United States, ‡Aero/Noise/Propulsion Laboratories, Boeing Co., Seattle, Washington 98124, United States, and §Department of Physics, Applied Physics and Astronomy, Rensselaer Polytechnic Institute, Troy, New York 12180, United States

ABSTRACT We present fabrication and characterization of macroscopic thin films of graphene flakes, which are functionalized with 1-pyrenecarboxylic acid (PCA) and are laminated onto flexible and transparent polydimethylsiloxane (PDMS) membranes. The noncovalently (π-stacked) functionalization of PCA allows us to obtain a number of unique optical and molecular sensing properties that are absent in pristine graphene films, without sacrificing the conducting nature of graphene. The flexible PCA−graphene−PDMS hybrid structure can block 70−95% of ultraviolet (UV) light, while allowing 65% or higher transmittance in the visible region, rendering them potentially useful for a number of flexible UV absorbing/filtering applications. In addition, the electrical resistance of these structures is found to be sensitive to the illumination of visible light, atmospheric pressure change, and the presence of different types of molecular analytes. Owing to their multifunctionality, these hybrid structures have immense potential for the development of versatile, low-cost, flexible, and portable electronic and optoelectronic devices for diverse applications.

KEYWORDS: graphene · functionalized graphene · graphene−polymer hybrid · UV absorbent material · transparent conducting films · sensors · photodetectors

Over the past few years, graphene has generated a great deal of interest in both fundamental and applied research areas.[1−3] Structurally, graphene is a single-atom-thick planar sheet of sp^2-bonded carbon atoms that are densely packed in a honeycomb crystal lattice. Its unique electronic structure, chemical bonding, and relatively defect-free crystalline order renders graphene with extremely high carrier mobility (~200 000 $cm^2\ V^{-1}\ s^{-1}$),[1] exceptional mechanical strength (Young's modulus ~1100 GPa,[2] fracture strength ~125 GPa),[2] and thermal conductivity (~5000 $W\ m^{-1}\ K^{-1}$).[3] These and other novel observations in graphene have generated quite a bit of excitement among researchers from diverse disciplines ranging from nanoelectronics[4,5] to composite materials[6,7] and energy applications.[8,9]

In the past, surface modification of graphitic materials such as carbon nanotubes and graphene with a variety of chemical groups has been demonstrated to be a novel method that can significantly enhance their functionalities.[10−12] In the case of graphene, a common method for achieving such functionalization is by a covalent modification of its surface, whereby the sp^2 symmetry is broken and carbon atoms are attached to hydroxyl groups or join with epoxide groups.[12] This chemical disruption of the graphitic order significantly affects the exceptional properties of graphene. For example, the process of chemical functionalization introduces impurities and disorder that are known to significantly deteriorate the conductive properties of graphene[12] and hence greatly diminishes their usefulness. An alternate method, involving functionalization through a benign π-stacking mechanism, allows selective functional groups to be attached without any disruption of the graphitic order. These functional groups can enable attractive new properties absent in pristine graphene, while retaining the mechanical, chemical, and electronic properties of graphene due to the noncovalent nature of its binding with the graphene surface. The latter method is in sharp contrast with the former and is clearly a better choice wherever the quality of graphene is crucial. In our previous work,[13] we had demonstrated how such a noncovalent functionalization could be achieved *via* π-stacking graphene with 1-pyrenecarboxylic acid (PCA). In this work, we describe hybrid structures of films of such functionalized graphene laminated on a flexible, inert,

*Address correspondence to x.an@neu.edu, s.kar@neu.edu.

Received for review September 15, 2010 and accepted December 21, 2010.

Published online January 13, 2011
10.1021/nn102415c

and transparent polymer surface and present interesting new results related to their optical and enhanced sensing properties.

The discovery that a single layer of chemically unmodified graphene (pristine graphene) absorbs a fundamental quantum of light ($\pi\alpha \approx 2.3\%$)[14] that is only dependent on the fine structure constant α ($\approx 1/137$) has generated immense interest in the fundamental nature of its optical properties. At the same time, it has opened up large possibilities for its application as the world's thinnest transparent conductive material, a fact that makes it immensely useful in many optoelectronic and photovoltaic applications. Experiments performed on pristine graphene as well as graphene produced by chemical reduction of graphene oxide[15−17] show very limited variation of their optical absorbance over large wavelength bands within the ultraviolet−visible (UV−vis) range. Compared to carbon nanotubes, the UV−vis spectrum of graphene is significantly featureless due to the smooth and monotonically increasing density of states of graphene near its Fermi level with marked absence of van Hove singularities. In carbon nanotubes, these singularities are a result of its 1D confinement (absent in 2D graphene) and are hallmarks of its electronic structure. Transitions between these singularities are directly responsible for the absorption peaks seen in the optical spectrum of carbon nanotubes. In the absence of such absorbance peaks, graphene by itself is incapable of acting as a wavelength-specific optically absorbent or filtering material within the UV−vis region.

In addition to its optical properties, the high-quality crystalline order of graphene renders it with extremely low electrical noise. This, combined with the fact that its conductance changes upon being doped and that it has very large specific surface area (calculated value, 2630 $m^2\ g^{-1}$),[18] makes it extremely attractive as a material for conductometric molecular sensing. Despite these advantages, however, pristine graphene shows little or no response to a variety of analyte molecules.[19] This is no surprise, since the covalent sigma bonds between the in-plane C atoms in graphene are completely satisfied, whereas the efficient pi-electron network on the surface leaves no available binding sites for analyte molecules to form any kind of chemical bonds that could potentially "dope" graphene and change its electrical conductance. However, it has been shown that even a monolayer of contaminants could vastly enhance its sensing abilities, and this has been attributed[19] to be the reason behind the demonstrated "single-molecule detection" by graphene. Hence, it stands to reason that a controlled type of surface functionalization will enable graphene to respond strongly in the presence of a certain type or category of analytes that can adhere to the said functional groups.

In our previous work, we have demonstrated a "molecular wedging" method for exfoliating graphene from graphite.[13] In this method, 1-pyrenecarboxylic acid (PCA), an amphiphilic molecule, is used as a molecular wedge to exfoliate graphene from graphite. This method retains the pristine nature of graphene; that is, it does not chemically modify graphene in any way. At the end of the exfoliation process, the graphene flakes are π-functionalized with PCA, which enables them to remain suspended stably in water. Although, in principle, the PCA molecules can be mostly removed from the graphene flakes by washing thoroughly in methanol, here we chose to retain the PCA molecules on the graphene surface, as they serve to provide a number of added functionalities as described below.

PCA, a well-known polyaromatic derivative, is a fluorophore that has sharp absorption peaks in the UV region.[20] This means that when exposed to UV light, PCA will absorb a significant amount of UV light. When attached to graphene, we find that PCA retains this extremely useful property. In addition, the dangling −COOH group of PCA provides sites for hydrogen bonding with polar analytes such as ethanol vapor,[13] which in turn could impact the electrical conductance of the PCA−graphene flakes, making them useful as conductometric sensors. To utilize these optical and sensing properties in macroscopically useful structures, we first fabricated thin films of overlapping PCA-functionalized graphene flakes and then laminated these films onto flexible, transparent substrates of polydimethylsiloxane (PDMS). In the past, carbon nanotube−polymer composites have been researched extensively for many applications that need the combination of unique electronic, optical, and mechanical properties of carbon nanotubes and polymer materials.[21−28] Graphene, as a new and outstanding member of carbon materials, will provide novel opportunities as composite materials in a variety of applications. Some groups have successfully made graphene−polymer composite structures with the potential ability for electrical applications.[29,30] Our method differs from these past reports in the fact that we use a benign surface functionalization of graphene in the hybrid structure to obtain unprecedented optical and sensing properties that graphene alone could not provide. The hybrid structures demonstrate large optical absorbance in the UV region, while remaining significantly transparent in the visible region of the optical spectrum. At the same time, its electrical resistance shows tremendous sensitivity to the presence of a large variety of polar molecules, including alcohols, ketones, and esters. We first present the fabrication of these hybrid structures, discuss their properties, and then summarize the implications of these findings.

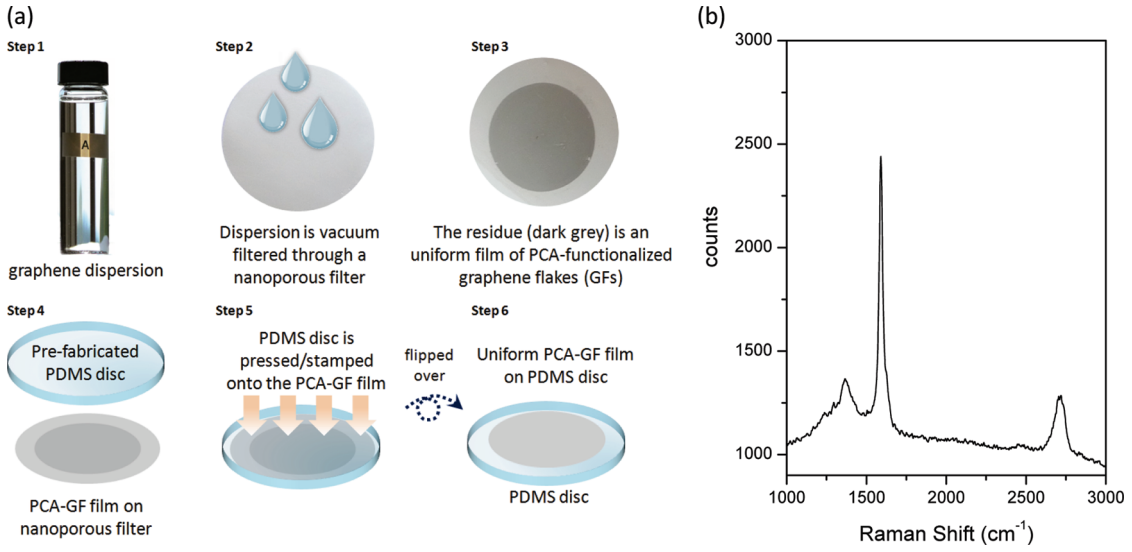

Figure 1. PCA−graphene−PDMS hybrid structures. (a) Scheme outlining the steps describing the fabrication process. (b) Raman spectrum of the PCA-functionalized graphene film showing characteristic peaks of few-layered graphene.

RESULTS AND DISCUSSION

Figure 1a schematically describes the process of the fabrication of graphene−polymer hybrid structures. An aqueous graphene dispersion, produced by our "molecular wedging" method,[13] contains PCA-functionalized graphene flakes that are a few hundred nanometers in size. This is vacuum filtered through a nanoporous cellulose-based membrane. The dispersion leaves a homogeneous gray or dark gray film on the surface of the membrane after it dries. Then, a prefabricated PDMS disk is pressed onto the surface of the graphene film on the cellulose. After the cellulose membrane is peeled off from the PDMS, a uniform graphene film is left on the surface of PDMS to produce the required graphene−polymer hybrid structure. The details will be explained in the Experimental Methods section. The obtained hybrid structure is partially transparent to the eye, is flexible, and can be cut into desired shapes and sizes and attached to external leads to form simple, flexible, multifunctional devices.

Since the dispersion used to fabricate the graphene film contains a mixture of monolayer (about 10%)[13] and few-layer graphene flakes, a similar layer-thickness distribution can be expected to be present in the film as well. Figure 1b is a Raman spectrum[31,32] taken on the graphene film on PDMS using an excitation wavelength of 532 nm. A strong peak indicative of the ordered graphitic crystal lattice known as the G-band was observed around 1584 cm^{-1}, which corresponds to the Raman-active doubly degenerate zone center E_{2g} phonon (in-plane optical mode) of sp^2-hybridized carbon, close to the Γ point. In addition, other peaks are observed at around 1350 cm^{-1} (corresponding to the D-peak or the first-order edge or defect-induced zone boundary phonons) and 2692 cm^{-1} (the D′-band related to second-order zone boundary phonons). The smaller peak at 2692 cm^{-1} in the Raman spectrum indicates the majority presence of few-layer graphenes. Together, these peaks represent the presence of graphene flakes in the hybrid structure.

We find that, to a good extent, the amount of graphene deposited on the PDMS surface increases with the amount of material that was previously deposited on the nanoporous membrane, i.e., by using different volumes of graphene dispersion while filtering. Figure 2a shows the optical images of graphene−polymer hybrid composite structures A, B, and C prepared using 5, 10, and 15 mL of graphene dispersion, respectively. To demonstrate their transparent nature, the hybrid structures have been placed on a printed Rensselaer logo. The transparent bulks are PDMS, and the gray or dark gray films on PDMS are graphene films. It can be seen that the contrast of graphene film changes slightly from gray to dark gray with the increase in volume of graphene dispersion used for the fabrication of these structures. Figure 2b shows the optical transmittance spectra within the UV−visible window (250−800 nm, using a Perkin-Elmer lambda-900 UV−vis−NIR spectrophotometer) on the PCA−graphene−PDMS hybrid structures A, B, and C. Table 1 summarizes the transmittance at different regions of the UV−vis spectrum. In the visible range from 400 to 800 nm, the average transmittance is varied from ~45% to 65% in the present set of samples. In comparison to their transmittance in the visible range, the transmittance in the ultraviolet region is extremely low, at 281 to 353 nm. As our previous work has shown,[13] these two wavelengths are fingerprints in the absorption spectrum of pure PCA. It is hence clear that the strong absorption of light at 281 and 351 nm in our structures is due to the noncovalently functionalized PCA on the surface of graphene. These results reveal that our

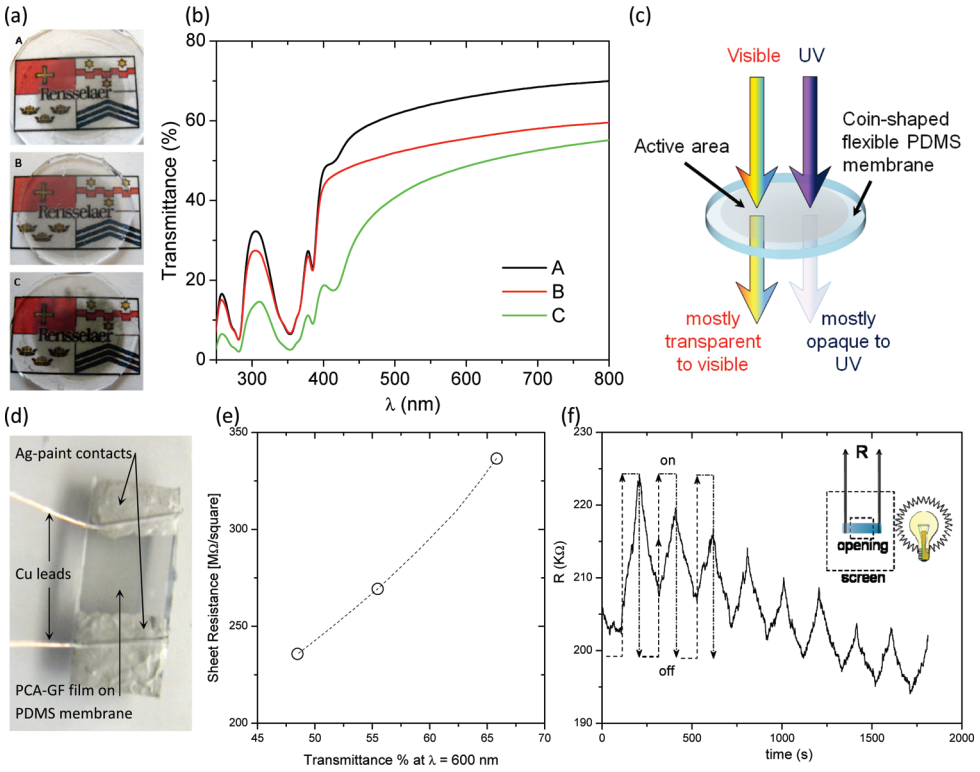

Figure 2. Optical properties of PCA−graphene−PDMS hybrid structures. (a) Digital optical images of three samples (A−C) with different degrees of graphene-film lamination. The discs were placed on a Rensselaer logo and photographed under the same lighting conditions for comparison. (b) UV−vis transmittance of the same samples, A−C. (c) Schematic describing the UV filtering action of these hybrid structures. (d) A rectangular piece of sample with electrodes attached for resistance measurement. (e) Sheet resistance of the samples with respect to their optical transmittance at 600 nm. (f) Variation of resistance *R* as a function of another sample when in the presence of an incandescent lamp that was periodically switched on and off. An opaque screen with a rectangular opening was used to mask the contact areas, and light was allowed to fall only on the graphene film, as shown.

TABLE 1. Transmittance of the Three Samples, A, B, and C, at Various Regions of the UV−Visible Spectrum

sample	average transmittance (%) 400−800 nm (visible)	transmittance (%) at 281 nm	transmittance (%) at 351 nm
A	64.2	4.63	6.37
B	54.6	4.71	6.64
C	44.9	1.87	2.51

graphene−PDMS hybrid structure can allow a significant amount of light to pass through in the visible region while selectively prohibiting transmittance in the UV region. This has been schematically shown in Figure 2c.

Figure 2d shows an optical photograph of a rectangular hybrid structure of a graphene film laminated on PDMS. Two external leads have been attached using a conductive silver paint, as shown. The functional area of the graphene film is around 0.5 × 0.5 cm^2. Since the graphene film is very thin, it is difficult to distinguish it from PDMS in this case. Such structures were used to measure the sheet resistance of PCA−graphene films of different thicknesses on PDMS, as well as to perform electrical tests under different conditions as described later on. Figure 2e shows the variation of sheet resistance of the PCA−graphene films on PDMS with different transmittance values. As expected, we find that the sheet resistance increases with increasing transmittance. These values of resistance are higher than that obtained in single flakes/continuous sheets of graphene. The high resistance can be ascribed to the high interfacial resistance between the numerous graphene flakes that form the microscopic structure of the film. In addition, the rough surface of PDMS may also add to nonplanar overlap of the flakes during the fabrication process. We are currently working on methods to decrease the sheet resistance, and this will be reported in the future. Despite this shortcoming, light absorption appears to have another interesting outcome in these samples: we find that our macroscopic structures are also photosensitive, with a reproducible change in overall conductivity in the presence of light. Figure 2f shows the variation of resistance as a function of time in a sample that has been isolated with a windowed screen (see inset of Figure 2f) and placed in front of an incandescent lamp. We see a periodic variation of its resistance with periodic switching on/off of the lamp. Our previous work has shown that

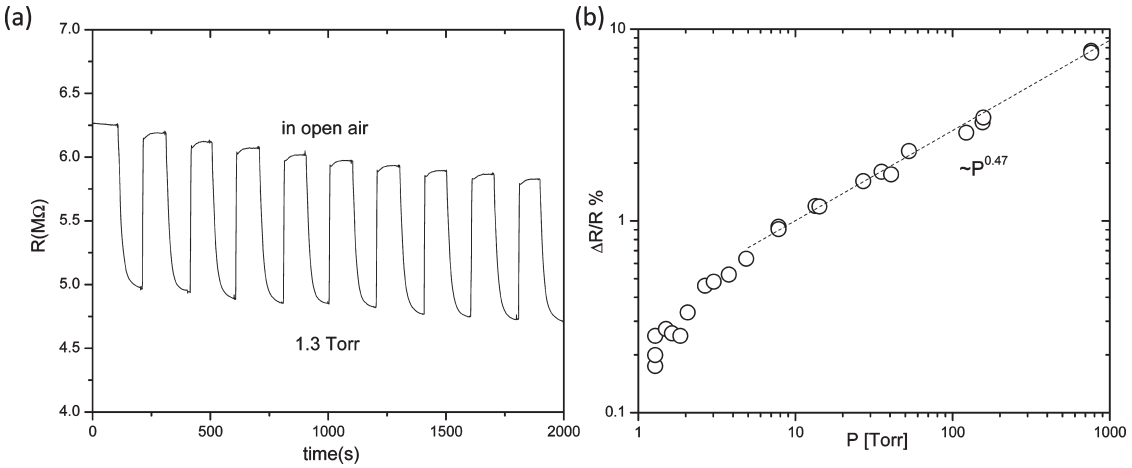

Figure 3. Atmospheric pressure sensing using PCA−graphene−PDMS hybrid structures. (a) Periodic variation of resistance in a hybrid structure in response to periodic change in pressure between 758 Torr (ambient atmospheric pressure) and 1.3 Torr. The resistance was found to decrease with a decrease in pressure. (b) Percentage change in resistance of the graphene films as a function of pressure. This change appears to follow a power-law trend at higher pressures.

these films have a negative temperature coefficient of resistance; that is, resistance decreases when the sample is heated.[13] In contrast, we find that the resistance of these films increases when the lamp is turned "on", indicating that the resistance change upon exposure to light is not due to "heating" of the sample from the lamp. The effect of gradual heating can be seen in the form of a steady decrease in overall resistance as a function of time, when the lamp has been switched "on" several times. The relative change in resistance of graphene flakes under illumination was found to be approximately 6%. The change in photoconductivity is found to be different from that previously reported for carbon nanotubes,[33,34] CdS nanoribbons,[35] GaN nanowires,[36] and ZnO nanowires,[37] where it has been demonstrated that photogenerated carriers result in the decrease of resistance with increasing incident light intensity. The exact mechanism of photodetection in our case is yet unclear, since electron−hole pair generation (in the presence of light) in graphene has time scales on the order of picoseconds,[38] whereas the response seen here is on the order of seconds. The UV absorbance of PCA is unlikely to produce this effect for similar reasons. It is possible that slow molecular desorption of oxygen[39] may be triggered by incident light, which could potentially cause the slow response seen in our samples. This would justify both the increase in resistance and the slow response seen in our experiments. However, detailed experimentation is required before further conclusions can be drawn in this regard.

Having discussed its various optical properties, we now turn to the molecular sensing aspect of our PCA−graphene−PDMS hybrid structures. In this case, PDMS plays the role of providing a stable substrate for the macroscopic PCA−graphene films. Molecular sensing can have a variety of uses, ranging from measurement of pressure of known gases to the detection of specific molecules. We first present the electrical properties of our PCA−graphene films with change in air pressure. Changing the ambient pressure will change the overall concentration of molecular constituents of air, and a reproducible and measurable change over a large range of pressures could be utilized in the fabrication of air pressure gauges or sensors. Air pressure sensors fabricated from graphene films will be low-cost, lightweight, and portable and will occupy a small volume. Such sensors would be useful in diverse applications in weather instrumentation, aircrafts, vehicles, and any other machinery that has pressure-related functionalities implemented.

Figure 3a shows the resistance change of a pressure sensor, made from a graphene hybrid structure (similar to the one shown in Figure 2d), as a function of time, while it is exposed to different air pressures. The test was performed in a vacuum chamber attached to pump/vent lines, and the pressure was controlled periodically through pumping/venting cycles and measured against a separate calibrated gauge. We find that the resistance of our pressure sensor decreases when the pressure of the measuring system is decreased to 1.3 Torr (base pressure of the pump) and recovers when the pressure of the system changes back to 758 Torr (ambient atmospheric pressure). The recovery was immediate, since the venting process is instantaneous. The decrease in resistance was initially rapid and then gradual, following the gradual approach toward the base pressure of our pump, at lower pressures. This indicated that our graphene pressure sensor responded quite rapidly to external changes in pressure. This has two immediate implications. First, on one hand, the change in electrical resistance is not an outcome of oxygen desorption as in case of our photodetection experiment, since that process involves large time scales, and desorption of oxygen causes an *increase* in resistance, quite the opposite of

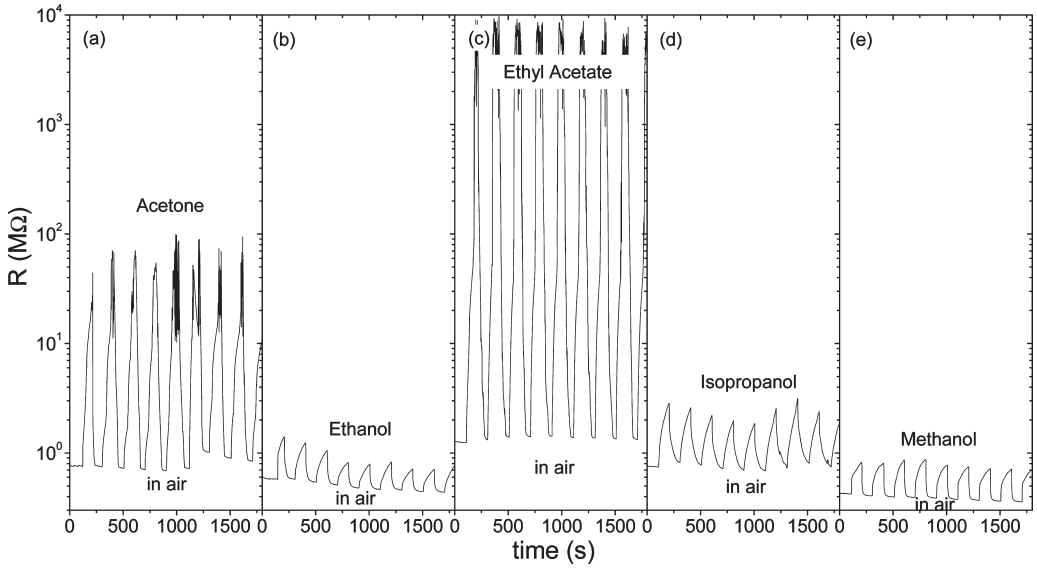

Figure 4. Periodic variations of sensor resistance in response to periodic exposure to saturated vapors of different organic solvents (see Table 1 for details). In each case, the resistance increases in the presence of the analyte vapors. The lower resistance values are those measured in air (in the absence of any analyte molecules).

what happens in this case. Similar arguments can be used to pre-empt any role of nitrogen or carbon dioxide,[19] two other major constituents of air. On the other hand, our previous work has shown that the presence of moisture can cause a small but reasonable increase in resistance in our PCA-functionalized graphene films.[13] Owing to their permanent dipole moment, water molecules can interact with the polar −COOH groups of PCA through a hydrogen-bonding mechanism, leading to an effective change in conductance that is consistent with both the rapid response of these sensors and the direction of resistance change. We believe that the decrease in sensor resistance with decreasing air pressure is due to the removal of water molecules in the pumping cycle (and *vice versa* for the venting cycle). Second, the rapid response makes it extremely useful for accurately monitoring rapid changes in ambient pressures, such as that required on aircrafts or vehicular stability control. To obtain their sensitivity, these sensors were tested over the entire range of pressure (1.25 Torr < P < 760 Torr). Figure 3b shows the percentage variation of response, $\Delta R/R$, at different controlled values of air pressure within this range. The percentage change is relative to the extrapolated value of resistance at $P = 1$ Torr. As the pressure is increased, so does the concentration of molecules in the chamber, and we find a monotonic increase in the sensor resistance up to a maximum of ~8% at atmospheric pressure. For 10 Torr < P < 760 Torr, the sensor resistance shows a power-law dependence on pressure (as shown in Figure 3b), making it easy to calibrate such sensors in this range. Compared to previous reports on carbon nanotube-based pressure sensors,[40,41] our pressure sensor is also easier to fabricate and has higher response to pressure change.

To further support our hypothesis that hydrogen bonding of PCA with polar molecules has an impact on the electrical resistance of the hybrid films, we have tested their behavior in the presence of organic solvent molecules that are known to have permanent dipole moments. Previously, we had presented preliminary results on sensors that were built on cellulose membranes.[13] However, cellulose is an organic compound and dissolves/degrades in most organic solvents or their vapors. This narrows down their usefulness, and hence they are unsuitable for testing against vapors of organic solvents such as acetone. The PDMS substrate used to build the present sensors overcomes this problem, since PDMS is an inert polymer and is insoluble in most organic solvents. Hence sensors fabricated from the present hybrid structures are extremely robust and could be used to test a wide range of molecular analytes.

Figure 4 show the resistance change of the PCA−graphene films in the presence of saturated vapors of acetone, ethanol, ethanol acetate, isopropyl alcohol, and methanol. We see the striking difference in their resistance in the presence of these analytes. Table 2 shows various experimental details, properties, and the percentage change in resistance seen in the presence of these analyte molecules. In comparison to the few percent change in resistance seen when the concentration of air (which comprises mostly nonpolar molecules except for water, as discussed before) was changed over orders of magnitudes, here we find that the percentage change in resistance is, in fact, orders of magnitude in size in the presence of a few to tens of percents of polar molecules. While at this point we do not fully comprehend why the presence of polar molecules will lead to such a large increase in its

TABLE 2. List of Polar Analytes Tested with Our PCA−Graphene Sensors, Concentrations Used, Molecular Properties, and Response

analyte	concentration % (v/v) in air	molecular weight[a] (g/mol)	dipole moment[a] (D)	response (ΔR/R)%
acetone	30.2	58.079	2.88 ± 0.03	5500 ± 925
ethanol	7.7	46.068	1.68 ± 0.03	85 ± 11
ethyl acetate	12.5	88.106	1.78 ± 0.09	547 063 ± 36 059
isopropyl alcohol	5.7	60.095	1.58 ± 0.03	209 ± 18
methanol	16.7	32.042	1.70 ± 0.02	100 ± 4.7

[a] These data were taken from ref 54.

resistance, we do note that the resistance recovers completely and instantaneously when the analyte is removed. This indicates that neither physisorption nor the formation of chemical bonds between the analytes and the PCA−graphene complex is occurring in the presence of the analyte, since the desorption process shows slower changes (as discussed before), and formation of chemical bonds will result in little or no recovery. This, in turn, means that resistance increase is not a "doping effect", which has been usually attributed to the cause for resistance change in pristine graphene in the past. We believe that this strikingly large response in the presence of polar molecules is due to the random trapping of a large number of dipoles near the surface of graphene due to the formation of hydrogen bonding between the analyte molecules and PCA. Our past work[42] with carbon nanotubes has shown that the presence of localized inhomogeneous electrostatic fields in the vicinity of nanotubes can open up large gaps in their density of states, resulting in orders-of-magnitude increase in their resistance. It is possible that the hydrogen-bonded polar molecules form a random array of strong, localized dipole fields near the parent graphene, and these random dipole potentials could affect the transport in graphene in a similar manner. In fact, experiments on bilayer graphene grown on SiC have shown that breakdown of layer symmetry due to formation of local dipoles can indeed lead to opening of band gaps in graphene.[43] The formation of hydrogen bonds is consistent with both the rapid response and complete recovery of the sensors, and we believe that trapping of local dipoles by the PCA molecules is possibly responsible for this large change in electrical resistance of graphene. In this preliminary report, it is not possible to completely ascertain this hypothesis, and systematic experimentation in conjunction with computational modeling is required to analyze the effect of dipole fields on graphene. We plan to investigate these issues in a comprehensive manner in the future. Regardless of the nature of the underlying mechanism, our observation opens up new methodologies for tailoring the sheet resistance of graphene-based devices and could be important for a number of electronic applications.

CONCLUSION

In conclusion, we have fabricated flexible multifunctional PCA−graphene−PDMS hybrid structures by transferring PCA-functionalized graphene films of various thicknesses onto PDMS substrates. The π-stacked (noncovalent) attachment of PCA on graphene enables us to obtain a variety of functionalities that are absent in pristine graphene, without sacrificing the conducting nature of graphene. The hybrid structures possess promising optical properties, in the form of UV absorption/suppression and photodetection, as well as molecular sensing properties, applicable in pressure sensors and molecular detectors. In particular, UV protection is a matter of great importance in the healthcare arena, especially in ophthalmology. Our simple methodology opens wider possibilities of tailoring wavelength-specific UV-absorbing materials, by selectively functionalizing the surface of graphene with other derivative of polyaromatic fluorophores, giving rise to UV absorption centered at different wavelength values, which is very useful for UV light filters.[44,45] PDMS is a transparent, inert, nontoxic, nonflammable, and biocompatible material similar to that used in contact lenses, and hence these laminated PDMS films find tremendous potential as UV protection in contact lenses and other optical devices such as microscopes, binoculars, and cameras. UV protection also has other industrial application such as protection of certain organic chemicals from degradation[46] or in textile industries.[47] Other possible uses include UV filters and coatings on windows in domestic, vehicular, military, and space applications.[44,45] In addition to its UV-suppressing property, the PCA molecules on graphene render them immensely sensitive to the presence of polar molecules. On one hand, this opens up a new method for tailoring the electronic properties of graphene films, which may have several fundamental and applied implications in graphene-based electronics. On the other hand, by tailoring the surface with different kinds of functional groups, this methodology may pave the

way for the development of a new generation of molecular sensors, which, again, could have numerous environmental, industrial, and military applications. Furthermore, we believe that the optimization of conductance of these hybrid structures can greatly enhance their potentials in fields where transparent conducting films are utilized, such as organic photovoltaic cells,[48,49] light-emitting diodes,[50,51] and electronic display.[52,53] These structures, hence, demonstrate a variety of functionalities and possess significant potential for the development of versatile, low-cost, flexible, and portable electronic and optoelectronic devices for diverse applications.

EXPERIMENTAL METHODS

The stable aqueous dispersion of noncovalently PCA-functionalized graphene is prepared by the "molecular wedging" method.[13] According to our previous work, the obtained PCA-functionalized graphene flakes are a few hundred nanometers in size, and the concentration of the dispersion is about 10 μm/mL. This graphene dispersion was vacuum filtered through cellulose membranes with pore size 25 nm. After the cellulose membranes dried, the dispersion gave a gray or dark (depends on how much dispersion used) contrast to the white membrane. The obtained graphene film on the cellulose membrane was then transferred onto the flexible polymer polydimethylsiloxane (PDMS) to get a graphene−polymer hybrid composite structure. The PDMS membrane was made by using a mixture of silicone elastomer base and silicone elastomer curing agent (10:1 in mass), which was put in an oven and dried under 60 °C after being sonicated for 10 min. This transferring step is carried out by stamping PDMS membranes onto the surface of a cellulose membrane overnight under the force of a 5 kg weight. The weight allows the PDMS to uniformly adhere to the top layer of the graphene flakes, which effectively laminates one side of the PDMS disk. After we peel the cellulose membrane off the PDMS, we obtain the flexible graphene−polymer hybrid composite structure. The hybrid composite structure can be cut into suitable shape and size and then attached to external leads by using silver paint on the two ends of the composite structure to fabricate multifunctional electrodes. The multifunctional electrodes made from the hybrid composite structure can be directly used as a controllable UV filter, transparent conducting films, photodetector, pressure sensor, and chemical sensor.

Acknowledgment. This work was supported by the Interconnect Focus Center New York at RPI, one of the five Focus Center Research Programs of Semiconductor Research Corporation. S.K. acknowledges NSF ECCS 0925708 for partial support.

REFERENCES AND NOTES

1. Bolotin, K. I. Ultrahigh Electron Mobility in Suspended Graphene. *Solid State Commun.* **2008,** *146*, 351–355.
2. Lee, C.; Wei, X.; Kysar, J. W.; Hone, J. Measurement of the Elastic Properties and Intrinsic Strength of Monolayer Graphene. *Science* **2008,** *321*, 385–388.
3. Balandin, A. A.; Ghosh, S.; Bao, W.; Calizo, I.; Teweldebrhan, D.; Miao, F.; Lau, C. N. Superior Thermal Conductivity of Single-Layer Graphene. *Nano Lett.* **2008,** *8*, 902–907.
4. Ritter, K. A.; Lyding, J. W. The Influence of Edge Structure on the Electronic Properties of Graphene Quantum Dots and Nanoribbons. *Nat. Mater.* **2009,** *8*, 235–240.
5. Freitag, M. Nanoelectronics Goes Flat Out. *Nat. Nanotechnol.* **2008,** *3*, 455–457.
6. Titov, A. V.; Kral, P.; Pearson, R. Sandwiched Graphene-Membrane Superstructures. *ACS Nano* **2010,** *4*, 229–234.
7. Eda, G.; Unalan, H. M.; Rupesinghe, N.; Amaratunga, G. A. J.; Chhowalla, M. Field Emission from Graphene Based Composite Thin Films. *Appl. Phys. Lett.* **2008,** *93*, 233502.
8. Wang, L.; Lee, K.; Sun, Y.; Lucking, M.; Chen, Z.; Zhao, J. J.; Zhang, S. Graphene Oxide as an Ideal Substrate for Hydrogen Storage. *ACS Nano* **2009,** *3*, 2995–3000.
9. Dimitrakakis, G. K.; Tylianakis, E.; Froudakis, G. E. Pillared Graphene: A New 3-D Network Nanostructure for Enhanced Hydrogen Storage. *Nano Lett.* **2008,** *8*, 3166–3170.
10. Wildgoose, G. G.; Abiman, P.; Compton, R. G. Characterising Chemical Functionality on Carbon Surfaces. *J. Mater. Chem* **2009,** *19*, 4875–4886.
11. Bourlinos, A. B.; Gournis, D.; Petridis, D.; Szabo, T.; Szeri, A.; Dekany, I. Graphene Oxide: Chemical Reduction to Graphite and Surface Modification with Primary Aliphatic Amines and Amino Acids. *Langmuir* **2003,** *19*, 6050–6055.
12. Ruoff, R. S.; Park, S. Chemical Methods for the Production of Graphenes. *Nat. Nanotechnol.* **2009,** *4*, 217–225.
13. An, X.; Simmons, T. J.; Shah, R.; Wolfe, C.; Lewis, K. M.; Washington, M.; Nayak, S. K.; Talapatra, S.; Kar, S. Stable Aqueous Dispersion of Non-Covalently Functionalized Graphene from Graphite and Their Multifunctional High-Performance Applications. *Nano Lett.* **2010,** *11*, 4295–4301.
14. Nair, R. R.; Blake, P.; Grigorenko, A. N.; Novoselov, K. S.; Booth, T. J.; Stauber, T.; Peres, N. M. R.; Geim, A. K. Fine Structure Constant Defines Visual Transparency of Graphene. *Science* **2008,** *320*, 1308.
15. Bao, Q.; Zhang, H.; Yang, J.; Wang, S.; Tang, D. Y.; Jose, R.; Ramakrishna, S.; Lim, C. T.; Loh, K. P. Graphene-Polymer Nanofiber Membrane for Ultrafast Photonics. *Adv. Funct. Mater.* **2010,** *20*, 782–791.
16. Liu, J.; Li, Y. L.; Li, Y. M.; Li, J. H.; Deng, Z. X. Noncovalent DNA Decorations of Graphene Oxide and Reduced Graphene Oxide toward Water-Soluable Metal-Carbon Hybrid Nanostructures *via* Self-Assembly. *J. Mater. Chem.* **2010,** *20*, 900–906.
17. Yang, L.; Deslippe, J.; Park, C. H.; Cohen, M. L.; Louie, S. G. Excitonic Effect on the Optical Response of Graphene and Bilayer Graphene. *Phys. Rev. Lett.* **2009,** *103*, 186802.
18. Stuller, M. D.; Park, S.; Zhu, Y.; An, J.; Ruoff, R. S. Graphene-Based Ultracapacitors. *Nano Lett.* **2008,** *8*, 3498–3502.
19. Dan, Y.; Lu, Y.; Kybert, N. J.; Luo, Z.; Johnson, A. T. C. Intrinsic Response of Graphene Vapor Sensors. *Nano Lett.* **2009,** *9*, 1472–1475.
20. Simmons, T. J.; Bult, J.; Hashim, D. P.; Linhardt, R. J.; Ajayan, P. M. Noncovalent Functionalization as an Alternative to Oxidative Acid Treatment of Single Wall Carbon Nanotubes with Applications for Polymer Composites. *ACS Nano* **2009,** *3*, 865–870.
21. Dresselhaus, M. S.; Dresselhaus, G.; Avouris, P. *Carbon Nanotubes: Synthesis, Structure, Properties, and Applications, Topics in Applied Physics 80*; Springer: New York, 2001.
22. Calvert, P. Nanotube Composites: A Recipe for Strength. *Nature* **1999,** *399*, 210–211.
23. Lahiff, E.; Ryu, C. Y.; Curran, C.; Minett, A. I.; Blau, W. J.; Ajayan, P. M. Selective Positioning and Density Control of Nanotubes within a Polymer Thin Film. *Nano Lett.* **2003,** *3*, 1333–1337.
24. Ahir, S. V.; Terentjev, E. M. Photomechanical Actuation in Polymer−Nanotube Composites. *Nat. Mater.* **2005,** *4*, 491–495.
25. Suhr, J.; Koratkar, N.; Keblinski, P.; Ajayan, P. M. Viscoelasticity in Carbon Nanotube Composites. *Nat. Mater.* **2005,** *4*, 134–137.

26. Koerner, H.; Price, G.; Pearce, N. A.; Alexander, M.; Vaia, R. A. Remotely Actuated Polymer Nanocomposites—Stress-Recovery of Carbon-Nanotube-Filled Thermoplastic Elastomers. *Nat. Mater.* **2004,** *3*, 115–120.
27. Hinds, B. J.; Chopra, N.; Rantell, T.; Andrews, R.; Gavalas, V.; Bachas, L. G. Aligned Multiwalled Carbon Nanotube Membranes. *Science* **2004,** *303*, 62–65.
28. Jung, Y. J.; Kar, S.; Talapatra, S.; Soldano, C.; Viswanathan, G.; Li, X.; Yao, Z.; Ou, F. S. Aligned Carbon Nanotube-Polymer Hybrid Architectures for Diverse Flexible Electronic Applications. *Nano Lett.* **2006,** *6*, 413–418.
29. Stankovich, S.; Dikin, D. A.; Dommett, G. H. B.; Kohlhaas, K. M.; Zimney, E. J.; Stach, E. A.; Piner, R. D.; Nguyen, S. T.; Ruoff, R. S. Graphene-Based Composite Materials. *Nature* **2006,** *442*, 282–286.
30. Ansari, S.; Giannelis, E. P. Functionalized Graphene Sheet-Poly (Vinylidene Fluoride) Conductive Nanocomposites. *J. Polym. Sci.: Part B: Polym. Phys.* **2009,** *47*, 888–897.
31. Ferrari, A. C.; Meyer, J. C.; Scardaci, V.; Casiraghi, C.; Lazzeri, M.; Mauri, F.; Piscanec, S.; Jiang, D.; Novoselov, K. S.; Roth, S. *et al.* Raman Spectrum of Graphene and Graphene Layers. *Phys. Rev. Lett.* **2006,** *97*, 187401-1–187401-4.
32. Graf, D.; Molitor, F.; Ensslin, K.; Stampfer, C.; Jungen, A.; Hierold, C.; Wirtz, L. Spatially Resolved Raman Spectroscopy of Single- and Few-Layer Graphene. *Nano Lett.* **2007,** *7*, 238–242.
33. Freitag, M.; Martin, Y.; Misewich, J. A.; Martel, R.; Avouris, P. H. Photoconductivity of Single Carbon Nanotubes. *Nano Lett.* **2003,** *3*, 1067–1071.
34. Wei, J. Q.; Sun, J. L.; Zhu, J. L.; Wang, K. L.; Wang, Z. C.; Luo, J. B.; Wu, D. H.; Cao, A .Y. Carbon Nanotube Macrobundles for Light Sensing. *Small* **2006,** *2*, 988–993.
35. Jie, J. S.; Zhang, W. J.; Jiang, Y.; Meng, X. M.; Li, Y. Q.; Lee, S. T. Photoconductive Characteristics of Single-Crystal CdS Nanoribbons. *Nano Lett.* **2006,** *6*, 1887–1892.
36. Han, S.; Jin, W.; Zhang, D.; Tang, T.; Li, C.; Liu, X.; Liu, Z.; Zhou, C. Photoconduction Studies on GaN Nanowire Transistors under UV and Polarized UV Illumination. *Chem. Phys. Lett.* **2004,** *389*, 176–180.
37. Cao, B. Q.; Matsumoto, T.; Matsumoto, M.; Higashihata, M.; Nakamura, D.; Okada, T. ZnO Nanowalls Grown with High-Pressure PLD and Their Applications as Field Emitters and UV Detectors. *J. Phys. Chem. C* **2009,** *113*, 10975–10980.
38. Xia, F.; Mueller, T.; Lin, Y. M.; Garcia, A.; Avouris, P. Ultrafast Graphene Photodetector. *Nat. Nanotechnol.* **2009,** *4*, 839–843.
39. Shi, Y.; Fang, W.; Zhang, K.; Zhang, W.; Li, L. J. Photoelectrical Response in Single-Layer Graphene Transistors. *Small* **2009,** *5*, 2005–2011.
40. Choi, J.; Kim, J. Batch-Processed Carbon Nanotube Wall as Pressure and Flow Sensor. *Nanotechnology* **2010,** *21*, 105502.
41. Gelamo, R. V.; Rouxinol, F. P.; Verissimo, C.; Vaz, A. R.; Bica de Moraes, M. A.; Moshkalev, S. A. Low-Temperature Gas and Pressure Sensor Based on Multi-Wall Carbon Nanotubes Decorated with Ti Nanoparticles. *Chem. Phys. Lett.* **2009,** *482*, 302–306.
42. Vijayaraghavan, A.; Kanzaki, K.; Suzuki, S.; Kobayashi, Y.; Inokawa, H.; Ono, Y.; Kar, S.; Ajayan, P. M. Metal-Semiconductor Transition in Single-Walled Carbon Nanotubes Induced by Low-Energy Electron Irradiation. *Nano Lett.* **2005,** *5*, 1575–1579.
43. Ohta, T.; Bostwick, A.; Seyller, T.; Horn, K.; Rotenberg, E. Controlling the Electronic Structure of Bilayer Graphene. *Science* **2006,** *313*, 951–954.
44. Su, G. B.; Zhuang, X. X.; He, Y. P.; Zheng, G. Z. A New Crystal of Ammonium Cobalt Nickel Sulfate Hexahydrate for UV Light Band-Pass Filter. *Opt. Mater.* **2008,** *30*, 916–919.
45. Su, G. B.; He, Y. P.; Li, Z. D.; Jiang, R. H.; Zhu, C. W.; Yang, S. F. Directional Solution Growth of Cylindrical α-$NiSO_4 \cdot 6H_2O$ Crystal. *J. Cryst. Growth* **2000,** *213*, 99–102.
46. Parejo, P. G.; Zayat, M.; Levy, D. Highly Efficient UV-Absorbing Thin-Film Coating for Protection of Organic Materials Against Photodegradation. *J. Mater. Chem.* **2006,** *16*, 2165–2169.
47. Paul, R.; Bautista, L.; Varga, M.; Botet, J. M.; Casals, E.; Puntes, V.; Marsal, F. Nano-Cotton Fabrics with High Ultraviolet Protection. *Text. Res. J.* **2010,** *80*, 454–462.
48. Tang, C. W. Two-Layer Organic Photovoltaic Cell. *Appl. Phys. Lett.* **1986,** *48*, 183–185.
49. Peumans, P.; Yakimov, A.; Forrest, S. R. Small Molecular Weight Organic Thin-Film Photodetectors and Solar Cells. *J. Appl. Phys.* **2003,** *93*, 3693–3723.
50. Aguirre, C. M.; Auvray, C. M. S.; Pigeon, R. S.; Izquierdo, P.; Desjardins, R. M. Carbon Nanotube Sheets as Electrodes in Organic Light-Emitting Diodes. *Appl. Phys. Lett.* **2006,** *88*, 183104-1–183104-3.
51. Zhang, D.; Koungmin, R.; Liu, X.; Polikarpov, E.; James, Ly.; Mark, E. T.; Zhou, C. Transparent, Conductive, and Flexible Carbon Nanotube Films and Their Application in Organic Light-Emitting Diodes. *Nano Lett.* **2006,** *6*, 1880–1886.
52. Baughman, R. H. Carbon Nanotubes—The Route toward Applications. *Science* **2002,** *297*, 787–792.
53. Li, J. F.; Hu, L.; Wang, L.; Zhou, Y.; Gruner, G.; Marks, J. T. Organic Light-Emitting Diodes Having Carbon Nanotube Anodes. *Nano Lett.* **2006,** *6*, 2472–2477.
54. *Handbook of Chemistry and Physics Online*; CRC Press, http://www.hbcpnetbase.com/. Accessed June 4, 2010.